

Tidal interaction of a rotating $1 M_{\odot}$ star with a binary companion

G.J. Savonije & M.G. Witte

Astronomical Institute ‘Anton Pannekoek’, University of Amsterdam, Kruislaan 403, 1098 SJ Amsterdam

received ?? ; accepted ??

Abstract. We calculate the tidal interaction of a uniformly rotating $1 M_{\odot}$ star with an orbiting companion at various phases of core hydrogen burning from the ZAMS to core hydrogen exhaustion. By using the traditional approximation we reduce the solution of the non-adiabatic oscillation equations for the tidal forcing of a rotating star to a one dimensional problem by solving a separate eigenvalue problem for the angular dependence of the tidal perturbations. The radial oscillation equations are then solved by using finite differencing on a fine grid with an implicit matrix inversion method like for stellar evolution calculations. We are able to identify resonances with gravity (g-)modes and quasi-toroidal (q-)modes with up to $\simeq 1000$ radial nodes in the more evolved stellar models. The resulting tidal torque is calculated down to low forcing frequencies close to corotation. For low tidal frequencies we find significant response due to inertial (i-)modes in the convective envelope. The inertial modes are damped by turbulent dissipation in the envelope and generate a relatively high torque-level in the low frequency region where the (retrograde) high radial order g-mode resonances become tidally inefficient due to their rotational confinement to the stellar equator and strong damping by radiative losses. For still lower retrograde forcing frequencies we find a large number of closely spaced weakly damped quasi-toroidal q-mode resonances. Our results indicate that effects related to stellar rotation can considerably enhance the speed of tidal evolution in low-mass binary systems.

Key words. Hydrodynamics– Stars: binaries– Stars: rotation– Stars: oscillation

1. Introduction

Spectroscopic observations show there is a fairly well determined orbital period below which main sequence binaries with solar-like stars have essentially circularized orbits. This circularization period appears to be $P_{\text{circ}} \simeq 11$ – 12 days (Duquennoy and Mayor 1991; Latham et al. 1992; Mathieu et al. 1992). In wider binary systems the tidal evolution is believed to be too slow to achieve circularization during the main sequence phase of solar-type stars. Since Zahn’s (1977) review of tidal effects there has recently been a renewed interest in tides in solar-type binary system, because the circularization times predicted by Zahn’s analysis are too long to explain the observations. Zahn considered the interaction of turbulent eddies with the hydrostatic *equilibrium tide*, i.e. the low frequency limit of the tidal response, as the dominant tidal mechanism in low mass stars with convective envelopes. Although this mechanism seems consistent with observed binary systems containing giant stars (Verbunt and Phinney 1995), it appears to fall short by orders of magnitude when compared with observed solar-type binary systems (e.g. Claret and Cunha 1997). Goodman and Oh (1997) also applied Zahn’s formalism and con-

cluded that it predicts a circularization period of only $P_{\text{circ}} \simeq 2.2$ days if one allows for the reduced efficiency of the viscous damping when the convective timescale of turbulent eddies is longer than the typical tidal forcing period. They find $P_{\text{circ}} \simeq 6$ days if one ignores this effect. Because the tidal torque scales as P_{orb}^{-4} , where P_{orb} is the orbital period, this forms a significant discrepancy with the observationally inferred $P_{\text{circ}} \simeq 11$ days.

Terquem et al. (1998, from now on T98) calculated the *dynamical tide* raised by a close companion on a non-rotating solar-type star. For dynamical tides the interaction between the tidal flow and the stellar normal modes of oscillation is taken into account (Cowling 1941). The stratification in low mass main sequence stars is complementary to that of massive stars and consists of a radiative core surrounded by a convective envelope. Near the boundary of the convective envelope the tides can excite g-modes in the radiative core, where radiative damping is relatively weak. Additional damping occurs in the convective envelope by the interaction of the tidal flow with turbulent eddies. T98 allowed for damping due to the interaction with these turbulent convective eddies by first order perturbation analysis, while radiative damping was treated by a WKB treatment of non-adiabatic terms.

They noted that the equilibrium tide applies to forcing frequencies much smaller than the Brunt-Väisälä frequency $|\mathcal{N}^2|^{\frac{1}{2}}$ (see below) and that for solar-type stars with relatively small values of $|\mathcal{N}^2|^{\frac{1}{2}}$ in the lower regions of the convective envelope the convective timescale is too long for essentially instantaneous adjustment to the tidal flow. Under these circumstances the equilibrium tide is a rather poor approximation for the tidal interaction and predicts a too strong effect. T98 found that for a fixed spectrum of normal modes in a non-rotating star the tidal evolution of solar-type binary systems is controlled essentially by the non-resonant dynamical tide. To explain the observed P_{circ} would require a viscosity that is $\simeq 50$ times larger than predicted by simple mixing length estimates. Goodman and Dickson (1998), in their WKB treatment of dynamical tides, considered non-linear damping of excited g-modes near the stellar centre but they estimate this cannot explain the discrepancy with the observations.

In T98 the stellar normal mode spectrum was considered fixed, i.e. for simplicity effects of stellar rotation and stellar evolution were ignored. However, in orbits with a significant eccentricity the tidal forcing is characterised not by one but by a spectrum of forcing frequencies which can potentially excite one or more of the normal modes in the binary stars. It is often argued that the chance of hitting a (narrow) resonance is small and that –when it happens– the enhanced tidal interaction rapidly moves the system through the resonance without much orbital evolution. This ignores the possibility of resonance locking. When stellar rotation is taken into account, the tides can excite both prograde (propagating in the direction of rotation) and retrograde (counter to rotation) oscillation modes, depending on the stellar rotation rate and orbital parameters. Excitation of prograde modes gives rise to spin-up (positive torques), while retrograde tidal forcing yields negative torques and spin-down. Calculations for massive binaries (Witte and Savonije 1999a,b, 2001, from now on WS99a; WS99b; WS01) indicate that often a weak high order prograde orbital harmonic is driven into resonance with a stellar gravity (g-)mode by the simultaneous action of a strong low frequency retrograde orbital harmonic which spins the star down, increasing the relative forcing frequency of the high orbital harmonic towards resonance. A similar driving effect can be caused by stellar evolution induced spin-down. The near-resonant weak prograde orbital harmonic tend to spin the star up, counteracting the retrograde driving ever more strongly when the peak of the resonance is approached. The two counteracting (retrograde and prograde) orbital harmonics then tend to lock each other at resonance with prolonged, considerably enhanced, tidal interaction. The effectiveness of the locking process is sensitive to the magnitude of the orbital eccentricity and to the low-frequency retrograde tidal forcing. Unfortunately, the low-frequency forcing excites high order (strongly damped) retrograde g-modes with short wavelengths which requires a very large number of mesh-points for finite difference calculations. The 2D oscillation

code (Savonije and Papaloizou 1997) which accounts for the full Coriolis force is not suited for the low frequency calculations with low-mass stars.

In this paper we calculate the fully non-adiabatic tidal interaction with a uniformly rotating solar-type star by applying the traditional approximation for which the ϑ -component of the stellar angular velocity is neglected. This is a reasonable approximation for low oscillation frequencies which simplifies the tidal problem significantly in that it allows a full separation of the tidal perturbations in the three spherical coordinates, like for a non-rotating star. Here we present tidal torque calculations (down to low forcing frequencies) for a uniformly rotating $1 M_{\odot}$ star at various stages of core hydrogen burning.

2. Basic tidal oscillation equations

We consider a uniformly rotating main sequence star with mass $M_s = 1 M_{\odot}$ and radius R_s . We assume the star’s angular velocity of rotation Ω_s to be much smaller than its break-up speed, i.e. $(\Omega_s/\Omega_c)^2 \ll 1$, with $\Omega_c^2 = GM_s/R_s^3$, so that effects of centrifugal distortion ($\propto \Omega_s^2$) may be neglected to a first approximation. We wish to study the response of this uniformly rotating star to a perturbing time-dependent tidal force. The Coriolis acceleration is proportional to Ω_s and we consider its effect on the tidally induced motions in the star. We use nonrotating spherical coordinates (r, ϑ, φ) , with the origin at the primary star’s centre, whereby $\vartheta = 0$ corresponds to its rotation axis which we assume to be parallel to the orbital angular momentum vector.

Let us denote the displacement vector in the star by $\boldsymbol{\xi}$ and perturbed Eulerian quantities like pressure P' , density ρ' , temperature T' and energy flux \mathbf{F}' with a prime. The linearised hydrodynamic equations governing the non-adiabatic response of the uniformly rotating star to the perturbing potential Φ_T may then be written as

$$\left[\left(\frac{\partial}{\partial t} + \Omega_s \frac{\partial}{\partial \varphi} \right) v'_i \right] \mathbf{e}_i + 2\Omega_s \times \mathbf{v}' = -\frac{1}{\rho} \nabla P' + \frac{\rho'}{\rho^2} \nabla P - \nabla \Phi_T, \quad (1)$$

$$\left(\frac{\partial}{\partial t} + \Omega_s \frac{\partial}{\partial \varphi} \right) \rho' + \nabla \cdot (\rho \mathbf{v}') = 0, \quad (2)$$

$$\left(\frac{\partial}{\partial t} + \Omega_s \frac{\partial}{\partial \varphi} \right) [S' + \boldsymbol{\xi} \cdot \nabla S] = -\frac{1}{\rho T} \nabla \cdot \mathbf{F}', \quad (3)$$

$$\frac{\mathbf{F}'}{F} = \left(\frac{dT}{dr} \right)^{-1} \left[\left(\frac{3T'}{T} - \frac{\rho'}{\rho} - \frac{\kappa'}{\kappa} \right) \nabla T + \nabla T' \right] \quad (4)$$

where κ denotes the opacity of stellar material and S its specific entropy. These perturbation equations represent, respectively, conservation of momentum, conservation of mass and conservation of energy, while the last equation describes the radiative diffusion of the perturbed energy flux. For simplicity we adopt the Cowling (1941) approximation, i.e. we neglect perturbations to the gravitational

potential caused by the primary's distortion. We also neglect perturbations of the nuclear energy sources and of convection.

Let us here consider the simplest case of a close binary system in which the orbit is circular with angular velocity ω and orbital separation D . The dominant tidal term of the perturbing potential is then given by the real part of

$$\Phi_{\text{T}}(r, \vartheta, \varphi, t) = fr^2 P_2^2(\mu) e^{i(\sigma t - 2\varphi)} \quad (5)$$

where $\sigma = 2\omega$ is the forcing frequency in the inertial frame, $\mu = \cos \vartheta$, $P_2^2(\mu)$ is the associated Legendre polynomial and $f = -\frac{GM_p}{4D^3}$, with M_p the companion's mass. After separating the φ -dependence, Eqs. (1–4) form a 2D problem in the (r, ϑ) meridional plane of the perturbed star. Let us now apply the traditional approximation in order to attain a considerable simplification of the tidal problem.

3. The traditional approximation

For $\Omega_s \neq 0$ the solutions of Eqs. (1–4) are no longer fully separable into r -, ϑ - and φ - factors due to the Coriolis force. However, in the traditional approximation separability is retained by neglecting the ϑ - component of the angular velocity (e.g. Unno et al. 1989). This is done because the radial motions are expected to be small in the stably stratified layers of the star, especially for low-frequency high-order g-modes. For this reason, it is thought to be a reasonable approximation for low oscillation frequencies. Furthermore, a spectrum of rotationally governed inertial modes as well as (quasi-)toroidal modes is also present in this approximation (Savonije et al. 1995).

When only the radial component of Ω_s is retained, the ϑ - and φ -components of the equation of motion can be written:

$$-\bar{\sigma}^2 \xi_\vartheta - 2i\Omega_s \bar{\sigma} \cos \vartheta \xi_\varphi = -\frac{1}{r\rho} \frac{\partial P'}{\partial \vartheta} - \frac{1}{r} \frac{\partial \Phi_{\text{T}}}{\partial \vartheta}, \quad (6)$$

$$-\bar{\sigma}^2 \xi_\varphi + 2i\Omega_s \bar{\sigma} \cos \vartheta \xi_\vartheta = \frac{im}{r\rho \sin \vartheta} P' + \frac{im}{r \sin \vartheta} \Phi_{\text{T}}. \quad (7)$$

We have expressed the velocity perturbations in terms of the displacement vector by the relation $\mathbf{v}' = i\bar{\sigma}\boldsymbol{\xi}$, with $\bar{\sigma} = \sigma - m\Omega_s$ the oscillation frequency in the corotating frame, where $m = 2$ in our study. We assume m to be always positive, whereby a retrograde oscillation (propagation direction counter to the sense of stellar rotation) corresponds with negative oscillation frequencies $\bar{\sigma}$.

3.1. Separation of variables

A separation of variables can be performed by writing, see Papaloizou and Savonije (1997):

$$\begin{aligned} \xi_\vartheta &= \sum_{n=1}^{\infty} \mathcal{F}_n(\vartheta) D_n(r) & \xi_\varphi &= \sum_{n=1}^{\infty} \mathcal{G}_n(\vartheta) D_n(r) \\ P' &= \sum_{n=1}^{\infty} X_n(\vartheta) W_n(r), \end{aligned} \quad (8)$$

with ξ_r , T' and ρ' having expansions of the same form as that for P' . Here \mathcal{F}_n , \mathcal{G}_n and X_n are functions of ϑ chosen to obey the relations

$$-\bar{\sigma}^2 \mathcal{F}_n - 2i\Omega_s \bar{\sigma} \cos \vartheta \mathcal{G}_n = -\frac{dX_n}{d\vartheta}$$

and

$$-\bar{\sigma}^2 \mathcal{G}_n + 2i\Omega_s \bar{\sigma} \cos \vartheta \mathcal{F}_n = \frac{im}{\sin \vartheta} X_n.$$

We obtain an equation for $X_n(\vartheta)$ by imposing the constraint

$$\frac{1}{\sin \vartheta} \frac{d(\sin \vartheta \mathcal{F}_n)}{d\vartheta} - im \frac{\mathcal{G}_n}{\sin \vartheta} = -\frac{\lambda_n}{\bar{\sigma}^2} X_n,$$

where λ_n is a constant. Then X_n must satisfy the second-order equation obtained from

$$\frac{1}{\sin \vartheta} \frac{dQ_n}{d\vartheta} + \frac{mx \cos \vartheta}{\sin^2 \vartheta} Q_n = X_n \left(\frac{m^2}{\sin^2 \vartheta} - \lambda_n \right) \quad (9)$$

with

$$Q_n = \frac{\sin \vartheta}{(1 - x^2 \cos^2 \vartheta)} \left(\frac{dX_n}{d\vartheta} - \frac{mx \cos \vartheta}{\sin \vartheta} X_n \right) \quad (10)$$

whereby $X_n(\vartheta)$ is an eigenfunction with λ_n the associated eigenvalue. The solution depends on the rotation parameter $x = 2\Omega_s/\bar{\sigma}$. The tidal problem we are interested in corresponds with even solutions of $X_n(\mu)$ with $\mu = \cos \vartheta$ and $m = 2$. For $\Omega_s = 0$ the functions $X_n(\vartheta)$ become the associated Legendre functions $P_{2n}^2(\cos \vartheta)$ with corresponding eigenvalues $\lambda_n = n(n+1)$. Normal modes of the rotating star correspond to normal modes of the non-rotating star with $n(n+1)$ replaced by any permissible λ_n .

Different $X_n(\vartheta)$ are orthogonal on integration with respect to $\mu = \cos \vartheta$ over the interval $(-1, 1)$. If the perturbing potential is expanded in terms of the X_n such that

$$\Phi_{\text{T}}(r, \vartheta) = \sum_{n=1}^{\infty} \mathcal{V}_n(r) X_n(\vartheta), \quad (11)$$

we find from (6) and (7) that

$$D_n(r) = \frac{1}{r\rho} W_n(r) + \frac{1}{r} \mathcal{V}_n(r). \quad (12)$$

This equation is exactly the same as in the non-rotating case. The same is true for the equation of continuity, except that $n(n+1)$ is replaced by λ_n . If we ignore the energy equation (see below) the tidal response will consist of a superposition of responses appropriate to non-rotating stars with $n(n+1)$ replaced by λ_n . Because the angular functions $X_n(\vartheta)$ are not spherical harmonics for non-zero rotation, all $n \equiv l$ are required in the superposition.

3.2. The modified oscillation equations

Once we have solved the above eigenvalue problem for λ_n the linearised equations which describe the non-adiabatic forced tidal oscillations for the n -th tidal component in

expansion (11) become a 1-dimensional (radial) problem by factoring out the common ϑ -dependence factor $X_n(\vartheta)$ of all occurring perturbations. The oscillation equations can now be expressed as

$$\bar{\sigma}^2 \rho \xi_r - \frac{dP'}{dr} + \frac{dP}{dr} \left(\frac{\rho'}{\rho} \right) = 2 \rho f r, \quad (13)$$

$$\frac{1}{\rho r^2} \frac{d(\rho r^2 \xi_r)}{dr} = -\frac{\rho'}{\rho} + \frac{\lambda_n}{\bar{\sigma}^2 r^2} \left[\frac{P}{\rho} \left(\frac{P'}{P} \right) + f r^2 \right], \quad (14)$$

$$\frac{P'}{P} - \Gamma_1 \frac{\rho'}{\rho} + \mathcal{A} \xi_r = i\eta \left[-\frac{1}{F r^2} \frac{d(r^2 F_r')}{dr} + \lambda_n \frac{\Lambda}{r^2} \left(\frac{T'}{T} \right) \right], \quad (15)$$

$$\frac{F_r'}{F} = \Lambda \frac{d}{dr} \left(\frac{T'}{T} \right) + (4 - \kappa_T) \frac{T'}{T} - (1 + \kappa_\rho) \frac{\rho'}{\rho} + \frac{\kappa_X}{X} \frac{dX}{dr} \xi_r, \quad (16)$$

where Γ 's represent Chandrasekhar's adiabatic coefficients, X the hydrogen abundance,

$$\Lambda = \left(\frac{d \ln T}{dr} \right)^{-1}, \quad \mathcal{A} = \frac{d \ln \rho}{dr} - \frac{1}{\Gamma_1} \frac{d \ln P}{dr},$$

$$\kappa_T = \left(\frac{\partial \ln \kappa}{\partial \ln T} \right)_\rho, \quad \kappa_\rho = \left(\frac{\partial \ln \kappa}{\partial \ln \rho} \right)_T, \quad \kappa_X = \left(\frac{\partial \ln \kappa}{\partial \ln X} \right),$$

$$\eta = -(\Gamma_3 - 1)F/(\bar{\sigma}P), \quad \text{with} \quad F = -\frac{4acT^3}{3\kappa\rho} \frac{dT}{dr}$$

the unperturbed radiative energy flux, and where the other constants have their usual meaning. The factor η is a characteristic radiative diffusion length. Note that the radiative diffusion introduces a factor i , so that the tidal perturbations are complex-valued which expresses the induced phase-lags with respect to the companion.

Although the energy equation is not separable, we have nevertheless simply replaced the $n(n+1)$ factor in the energy equation for a non-rotating star by λ_n (eq. 15) to approximately take the horizontal radiative diffusion into account. It appeared that the inclusion (exact for non-rotating stars) or non-inclusion of this term yields almost the same values for the tidal torque, even when $|\lambda|$ becomes large at low retrograde forcing frequencies.

Finally, the oscillation equations are complemented by the linearised equation of state

$$\frac{P'}{P} = \left(\frac{\partial \ln P}{\partial \ln T} \right) \frac{T'}{T} + \left(\frac{\partial \ln P}{\partial \ln \rho} \right) \frac{\rho'}{\rho} + \left(\frac{\partial \ln P}{\partial \ln \mu_a} \right) \frac{\mu'_a}{\mu_a} \quad (17)$$

where μ_a is the mean atomic weight of the stellar gas. In radiative layers we assume convection of oscillatory stellar material without any diffusion, so that

$$\frac{\mu'_a}{\mu_a} = -\frac{d \ln \mu_a}{dr} \xi_r.$$

3.3. Turbulent viscosity

The tidal oscillations are expected to be influenced by the turbulent convective motions in the stellar envelope. We describe these interactions in a heuristic way by means of a simple mixing length approximation for turbulent viscosity. To this end we add in the convective envelope a radial viscous force density

$$f_{r,\text{visc}} = \frac{i\bar{\sigma}}{r^2} \frac{\partial}{\partial r} \left(\rho \nu r^2 \frac{\partial \xi_r}{\partial r} \right)$$

to the equation of motion (13), with ν a turbulent viscosity coefficient. In order to enable comparison we adopt the same form for the turbulent viscosity coefficient as T98:

$$\nu = \frac{L^2}{\tau_{\text{con}}} \left[1 + \left(\tau_{\text{con}} \frac{\bar{\sigma}}{2\pi} \right)^s \right]^{-1} \quad (18)$$

where L is the mixing length, taken to be twice the local pressure scale height, $\tau_{\text{con}} = |\mathcal{N}^2|^{-\frac{1}{2}}$ the characteristic convective timescale with $\mathcal{N}^2 = -g\mathcal{A}$ the square of the Brunt-Väisälä frequency, whereby g denotes the local acceleration of gravity. The reduced efficiency of the turbulent damping of high frequency oscillations by the slow convective motions is taken approximately into account by the factor in square brackets, where we adopt $s = 2$. See Goldreich and Keeley (1977), Goldman and Mazeh (1991) and Goodman and Oh (1997) for a discussion. The maximum value of the adopted viscosity coefficient ν is attained near the lower boundary of the convective envelope. In the stellar models used this maximum value ranges from a few times 10^{13} to slightly more than 10^{15} in cgs units, whereby the latter value is reached for low forcing frequencies. Both the radiative and turbulent damping induce a phase lag of the tidal response with respect to the forcing by the companion and that gives rise to the tidal torques we are interested in. The torque-values both in between and near resonances are sensitive to the adopted turbulent viscosity law.

3.4. The tidal torque

The tidal torque integral corresponding with the n -th term of the expansion (11) can be expressed as:

$$\mathcal{T}_n(\bar{\sigma}, \Omega_s) = \pi \zeta_n^2 f \int_0^{R_s} \text{Im} [\rho'_n(r)] r^4 dr \quad (19)$$

where π results after the integration over φ , f is the constant in the tidal potential defined by Eq. (5), Im stands for imaginary part, and

$$\zeta_n^2 = \frac{\left[\int_{-1}^1 P_2^2(\mu) X_n(\mu) d\mu \right]^2}{\int_{-1}^1 X_n^2(\mu) d\mu}. \quad (20)$$

ζ_n is an overlap integral of the eigenfunctions $X_n(\mu)$ with $P_2^2(\mu)$, the associated Legendre polynomial describing the μ variation of the dominant $l = m = 2$ tide. The tidal

torque is proportional to ζ_n^2 , which for $n = 1$ and $\Omega_s \rightarrow 0$ attains the value 48/5.

The tidal torque follows by multiplying \mathcal{T}_n by the factor $m = 2$. Once we have, for a given forcing frequency $\bar{\sigma}$ and stellar angular rotation speed Ω_s , first solved the $\lambda_n(x)$ eigenvalue problem and subsequently the radial oscillation Eqs. (13–16), the resulting $\rho'_n(r)$ can be substituted in the above integral to evaluate the tidal torque.

4. Solution method

4.1. Determination of angular eigenvalue $\lambda_n(x)$

For a given stellar rotation frequency Ω_s and forcing frequency $\bar{\sigma}$ the eigenvalues λ_n can be determined by numerically integrating the two ordinary differential Eqs. (9) and (10). We have used a shooting method with fourth order Runge-Kutta integration with variable stepsize (e.g. Press et al. 1992). To this end we rewrite the equations as

$$\frac{dX_n}{d\mu} = -\frac{mx\mu}{1-\mu^2} X_n - \left(\frac{1-x^2\mu^2}{1-\mu^2} \right) \mathcal{Q}_n, \quad (21)$$

$$\frac{d\mathcal{Q}_n}{d\mu} = -\left(\frac{m^2}{1-\mu^2} - \lambda_n \right) X_n + \frac{mx\mu}{1-\mu^2} \mathcal{Q}_n \quad (22)$$

where the factor $x = 2\Omega_s/\bar{\sigma}$ expresses the importance of stellar rotation.

To enable integration away from $\mu = 1$ it is convenient to write $X_n(\mu) = (1-\mu^2)^{\frac{m}{2}} Y_n(\mu)$ and expand $Y_n(\mu)$ in a power series $Y_n = c_0 + c_1(\mu-1) + c_2(\mu-1)^2 + \dots$ which can be substituted in Eqs. (21) and (22) to determine the coefficients c_k . We use c_0 as a free scaling parameter and express coefficients c_1 to c_4 in terms of c_0 , x and the unknown eigenvalue λ_n . \mathcal{Q}_n can then be expressed in terms of Y_n as

$$\mathcal{Q}_n = \frac{(1-\mu^2)^{\frac{m}{2}}}{1-x^2\mu^2} \left[m\mu(1-x) Y_n - (1-\mu^2) \frac{dY_n}{d\mu} \right].$$

For the even (in μ) $m = 2$ solutions the boundary conditions are $X_n = 0$ at $\mu = 1$ and $\mathcal{Q}_n = 0$ at $\mu = 0$. We can now integrate equations (21)–(22) from $\mu = 1 - \epsilon$ (with $\epsilon = 10^{-4}$) to $\mu = 0$ with an estimated value for the eigenvalue λ_n . We iterate by adjusting λ_n until the integrated value for \mathcal{Q}_n is sufficiently close to zero for $\mu = 0$.

4.2. Numerical solution of radial oscillation equations

Once $\lambda_n(x)$ is determined by means of the above numerical method the radial oscillation Eqs. (13–16) can be solved for the same value of $\bar{\sigma}$ after prescribing the usual boundary conditions $\xi_r = F' = 0$ at the stellar centre and by requiring that the Lagrangian perturbations at the stellar surface obey: $\delta P' = 0$ and $\delta F'/F = 4\delta T'/T$ (Stefan's law). By transforming the differential equations into algebraic equations by means of finite differences on a spatial mesh and applying matrix inversion similar to standard Henyey schemes for stellar evolution the radial equations can be solved (e.g. Savonije and Papaloizou 1983). The

viscous diffusion term requires three-level finite differencing. It appears that, because of the short wavelength of the tidal response for low forcing frequencies $\bar{\sigma}$ one needs a large number of meshpoints for a solar-type star: we have used 5000 radial points. The 2D oscillation code (Savonije and Papaloizou 1997) which takes the Coriolis force fully into account would require unrealistically long integration times for such a fine radial grid in combination with an adequate resolution in ϑ . In order to obtain consistent results for the resonances we have used the traditional approximation also outside the low frequency inertial range (although in Figure 2 we only show results for $|x| < 1$).

5. Stellar models

We constructed the unperturbed stellar models for the solar-type star with a recent version (Pols et al. 1995) of the stellar evolution code developed by Eggleton (1972). The models represent a spherical main sequence star of 1 M_⊙ with chemical composition given by various values of the central hydrogen abundance X_c and $Z = 0.02$. The model was constructed by using the OPAL opacities (Iglesias and Rogers 1996). Fig. 1 shows a frequency related to the Brunt-Väisälä frequency \mathcal{N} , namely $\nu_{\text{BV}} = \text{sign}\mathcal{N}\sqrt{|\mathcal{N}|}$ in units of the stellar break-up speed Ω_c versus mesh point number for both an unevolved stellar model and for a model near the end of core hydrogen burning. In the latter model the square of the Brunt-Väisälä frequency has become quite large in the contracted helium core. The radiative core, where the tidal oscillations occur, is made to contain roughly 4000 meshpoints in order to resolve the short wavelength response for low forcing frequencies.

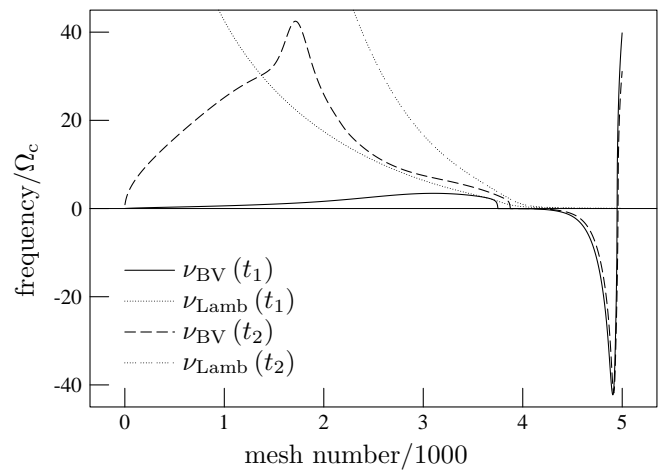


Fig. 1. The modified Brunt-Väisälä frequency $\nu_{\text{BV}} = \text{sign}\mathcal{N}\sqrt{|\mathcal{N}|}$ and Lamb-frequency in units of the stellar break-up speed Ω_c versus meshpoint number for (t_1 : 0.15 Gyr) an unevolved 1 M_⊙ model, and (t_2 : 11 Gyr) for a stellar model with central hydrogen abundance $X_c \simeq 0$.

6. Results

6.1. The solution for the eigenvalues λ_n

We only show the solution of the eigenvalue problem in the the low-frequency inertial regime, for which the absolute value of the rotation parameter $x = 2\Omega_s/\bar{\sigma}$ is larger than unity. Negative x -values correspond to retrograde, positive values to prograde forcing.

6.1.1. g-mode solutions

The calculated positive eigenvalues λ_n , with $n = 1$ to 5, are shown as a function of $1/x$ in Fig. 2a. For large values of $|1/x|$ the eigenvalues λ_n approach the values $l(l+1)$ (with $l=2n$), corresponding to vanishing rotation. The values for λ_1 are consistent with those calculated in Papaloizou and Savonije (1997). It can be seen that rotational effects become strong when $|1/x| \rightarrow 0$, i.e. when the oscillation frequency becomes small compared to the angular speed of the star.

The large values for λ_n for $|x|^{-1} \rightarrow 0$ are associated with eigenfunctions X_n which attain small values for $1 \geq \mu \gg |x|^{-1}$, while the peak(s) shift(s) to $\mu = 0$. This corresponds to the confinement of g-modes towards the stellar equator due to strong Coriolis effects near the poles for small oscillation frequencies. For the lowest eigenvalue this effect is strongest for the retrograde g-modes. Fig. 2c shows the angular overlap integral (20) $^{10}\log[\zeta_n^2]$ as a function of $1/x$ for $\lambda_n > 0$. Due to the equatorial confinement of the g-modes their coupling to the tides becomes weak when $|1/x|$ becomes small, with strongly reduced values of ζ_n . The latter effect is enhanced due to the fact that the retrograde solutions have one node more in the ϑ direction than the corresponding prograde solutions.

6.1.2. r and q-mode solutions

For $-1/6 < x^{-1} < 0$ there are solutions with small eigenvalues, see Fig. 2a. The solution with $\lambda_n = 0$ is a purely toroidal oscillation with frequency corresponding to $x = -6$. This solution corresponds to the class of r-modes (Papaloizou and Pringle 1978) with frequencies

$$\bar{\sigma}_r = -\frac{2m\Omega_s}{l(l+1)}.$$

For the lowest order $l = 3$ (which couples to the dominant $l = m = 2$ tide) this frequency coincides with $1/x = -1/6$. In previous papers (WS99a; WS99b; WS01) we loosely called the quasi-toroidal modes (with associated small but non-zero values of λ_n) also r-modes, but here (see section 6.5) we have identified these modes up to high radial order for which the non-toroidal character becomes significant and we denote them as *q-modes*. Like g-modes, the peak(s) of the eigenfunctions for q-modes shift to small values of μ when $x^{-1} \rightarrow 0$, although the equatorial confinement is less pronounced. It can be seen in Fig. 2c that the q-modes couple effectively to the $l = m = 2$ tide, with the angular overlap integral $\zeta^2 \simeq 10$.

6.1.3. i-mode solutions

Solutions with $\lambda_n < 0$ are associated with rotationally governed *inertial* i-modes which can propagate in the approximately adiabatic convective envelope. Fig. 2b shows the absolute value of the eigenvalues associated with inertial solutions for $m = 2$ and with the adopted even symmetry in μ for the eigenfunctions X_n . When $|x|^{-1} \rightarrow 1$ the eigenfunctions of the i-solutions become more and more confined to the stellar poles, i.e. the coupling with the tide decreases when the effect of rotation becomes weaker (see Fig. 2d). The eigenvalues for the prograde i-solutions vanish when $x^{-1} \rightarrow 0$, while the eigenvalues for retrograde i-solutions tend to zero for small, but finite values of $|x|^{-1}$. The eigenvalue corresponding to the fundamental inertial solution drops in fact to zero for $1/x \rightarrow -1/6$. At this point the fundamental inertial solution connects to the toroidal r-solution. The prograde solutions have one node more in the ϑ direction than the corresponding retrograde solutions.

6.2. The eigenfrequencies: effects of stellar evolution

By substituting the calculated values for the angular eigenvalue λ_1 (for the given value of $x = 2\Omega_s/\bar{\sigma}$) in Eqs. (13)–(16) and solving these equations numerically for a range of forcing frequencies $\bar{\sigma}$, the resonances with stellar oscillation modes are readily found. By doing this for several stellar input models, at various phases of core hydrogen burning, one can follow the evolution of the normal mode resonances of the 1 M_⊙ star from the ZAMS to the end of core hydrogen burning. We have calculated the resonances for a non-rotating star, as well as for a star rotating at $\Omega_s = 0.1$ and 0.2 (in units of Ω_c). Figs. 3a–3d show the evolution of the resonance frequencies for prograde and retrograde g-modes for stellar rotation speeds $\Omega_s = 0.1$ and 0.2, as the 1 M_⊙ star evolves away from the ZAMS. In both cases the g-mode frequencies increase with age, as is expected from the fact that the stellar core contracts, so that the acceleration of gravity increases in the propagation region of the modes. We also find that the retrograde g-modes have higher resonance frequencies (in absolute value) than their prograde counterparts.

Figs. 3e and 3f show the more complex evolution of the quasi-toroidal q-modes when the star evolves away from the ZAMS. The frequency of toroidal modes is proportional to the rotation speed Ω_s . When the star evolves away from the ZAMS its radius increases, at first slowly, but near the end of core hydrogen burning more quickly. Rotation at fixed Ω_s/Ω_c thus means that the stellar rotation rate assumed for this figure slows in fact down with age because our frequency unit Ω_c decreases when the star expands. This tends to bring down the mode frequencies with age, as is indeed the case for the low radial order q-modes. However, the higher radial order q-modes correspond with larger eigenvalues λ_1 and thus with an increasing non-toroidal character as the radial node number k rises, for which buoyancy effects become important.

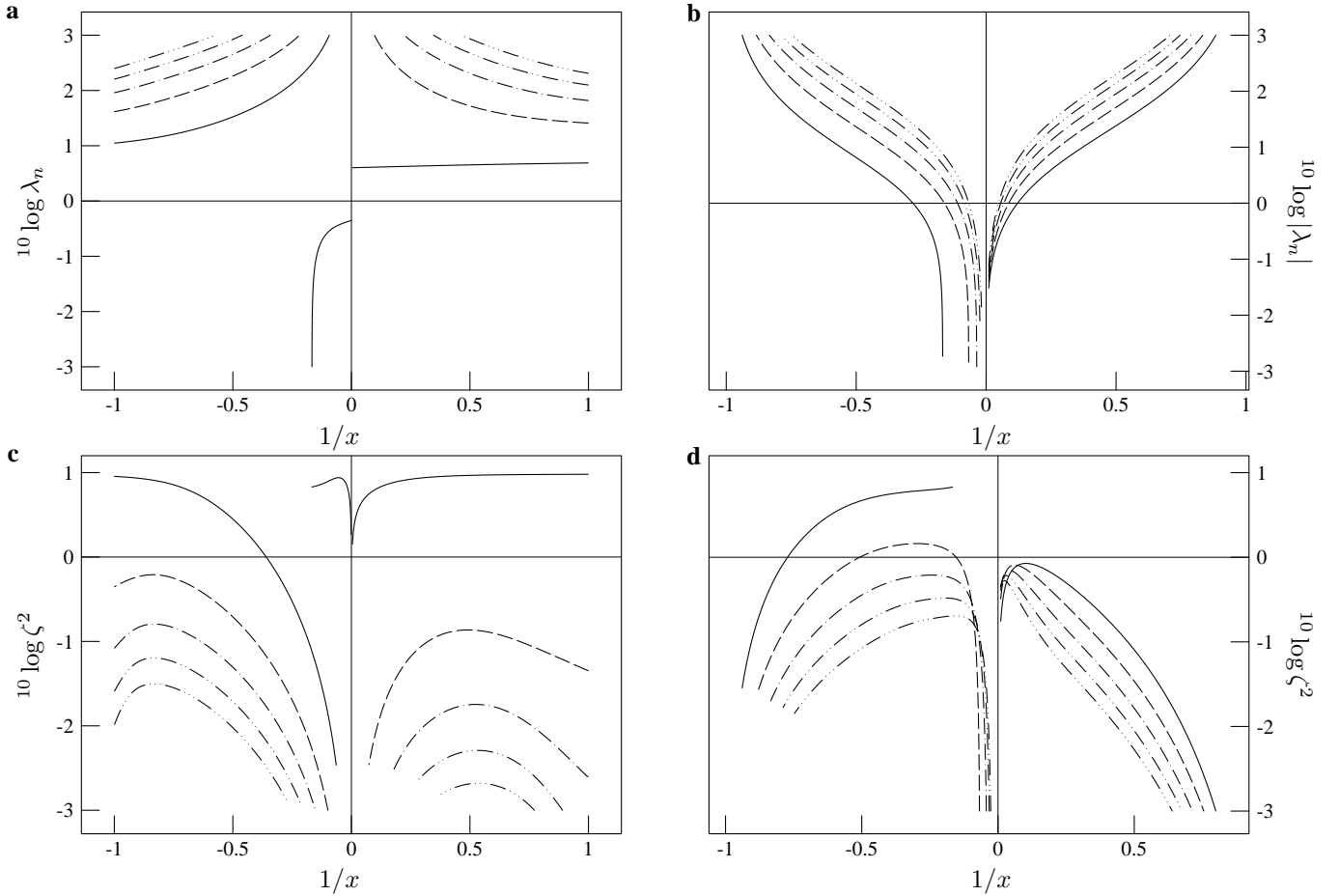


Fig. 2. **a** The calculated positive eigenvalues λ_n (for $n = 1$ to 5) versus $1/x = \bar{\sigma}/(2\Omega_s)$ for $m=2$, corresponding to eigenfunctions with even symmetry in μ . The full curves correspond to $n = 1$, the uppermost curves to $n = 5$. **b** The same as panel a but now for the negative eigenvalues. **c** The square of the tidal angular overlap integral ζ_n for $\lambda_n > 0$ versus $1/x$ with same line coding for $n=1$ to 5 . **d** The square of ζ_n for $\lambda_n < 0$ versus $1/x$ with same line coding for $n=1$ to 5 .

This explains why the frequency of the high order q-mode resonances increase with age, like g-modes. Comparing Figs. 3e and 3f shows that the resonance frequencies of low-order q-modes do indeed scale with Ω_s , and less so for the high order q-modes.

6.3. Determination of the tidal torque

Although the expansion (11) should be made over all n values, the strength of the tidal coupling decreases (Figs. 2c-d) rapidly for higher orders, so that we will from now on consider only the first eigenvalue λ_1 , and ignore the intrinsically weaker coupling of the higher order eigenfunctions.

For a given forcing frequency $\bar{\sigma}$ and stellar spin rate Ω_s we first determine $\lambda_1(x)$ and substitute this in the set of Eqs. (13–16). After solving these equations (section (4.2) and substituting the obtained imaginary part of ρ' in the torque integral (19) the tidal torque can be evaluated. The calculations are done for a perturbing companion of $1 M_{\odot}$ in *circular* orbit with binary separation $D = 4R_s$, i.e. for a *fixed* ratio of R_s/D . The values for the torque integral

\mathcal{T}_1 have to be multiplied by a factor $m = 2$ to get the tidal torque T .

The tidal torque on a non-synchronously rotating solar-type star in a given binary system with a companion of mass M_p in a circular orbit with arbitrary orbital separation D is then found from

$$T(\bar{\sigma}) = m \left(\frac{M_p}{M_{\odot}} \right)^2 \left(\frac{4R_s}{D} \right)^6 \mathcal{T}_1(\bar{\sigma})$$

where, for a stellar model with $X_c \simeq 0.4$ and a given value of $\bar{\sigma} = \sigma - m\Omega_s$ with $m = 2$, \mathcal{T}_1 can be read from Figs. 4 to 6.

6.4. Comparison with T98's calculation

To check our results we have compared some of our torque-values for the non-rotating case with those of T98, as there exist no detailed results for rotating stars to compare with. Table 1 gives some results of both calculations for three different circular orbits with periods of 4.2, 8.5 and 12.4 days. In the table we have scaled our results to those of T98, i.e. we use their normalisation of the tidal

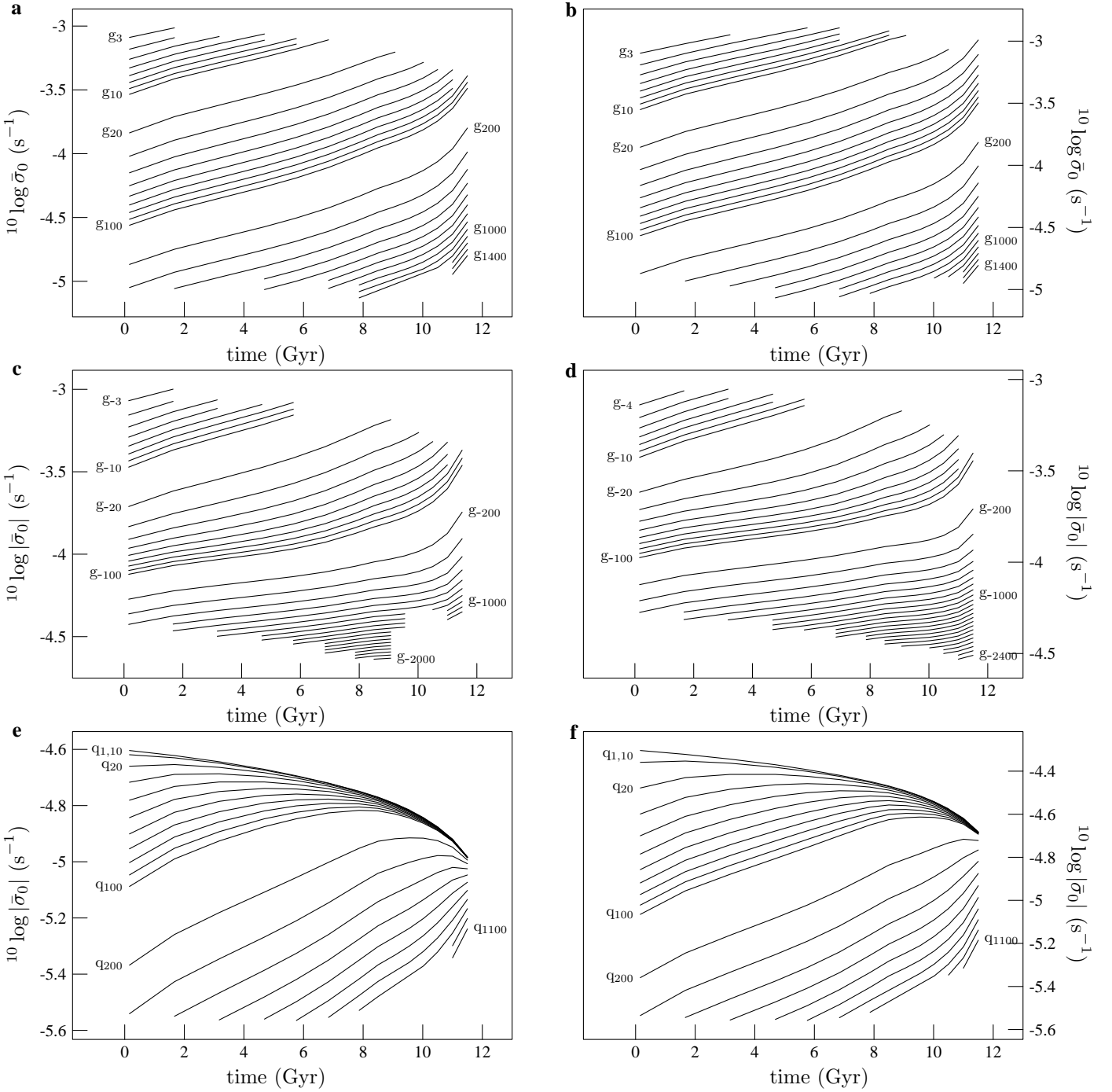


Fig. 3. The variation of resonance frequencies σ_0 corresponding to $\lambda_1 > 0$ with stellar evolution. **a** and **b** The prograde g-modes for rotation rate $\Omega_s = 0.1$ and 0.2 , respectively. **c** and **d** The retrograde g-modes for rotation rate $\Omega_s = 0.1$ and 0.2 . **e** and **f** The quasi-toroidal q-modes for rotation rate $\Omega_s = 0.1$ and 0.2 .

torques as in their Fig. 2. After comparing their torque values with our results for non-rotating stars we conclude that the two calculations yield quite similar results.

6.5. Torque spectra for $\lambda_1 > 0$ (g- and q-modes)

After repeating the torque calculation procedure for a wide range of frequencies ($|\bar{\sigma}| \leq 1$, where all frequencies stated without units are in units of the critical rotation

rate Ω_c), we end up with a number of torque spectra, like the one shown in Fig. 4 for $\Omega_s = 0.1$ and $X_c = 0.4$. Note that the actual height of the resonances depends on the adopted turbulent viscosity law for the convective regions and on the amount of turbulent overshooting. We have assumed a Gaussian decay of the viscosity coefficient beyond the convection boundaries with a decay length of 0.5 pressure scale height.

Table 1. Comparison of calculated torque values: the upper values are from T98, while the lower values correspond to the calculations presented here. T_{peak} and T_{off} are the torque values at the resonance peaks considered, and for neighbouring off-resonant frequencies, respectively. The middle column gives the relative FWHM of the resonance peaks.

P (d)	T_{peak} (cgs)	$\Delta\sigma/\sigma$	T_{off} (cgs)
4.2	3.2×10^{38}	3×10^{-6}	4×10^{35}
	3.4×10^{38}	7×10^{-6}	7×10^{35}
8.5	2.8×10^{35}	4×10^{-5}	6×10^{34}
	3.6×10^{35}	4×10^{-5}	5×10^{34}
12.4	6.3×10^{33}	2×10^{-4}	5×10^{33}
	1.5×10^{34}	2×10^{-4}	7×10^{33}

The high frequencies near $|\bar{\sigma}| = 1$ will never occur in normal binaries with solar-type stars, but part of the higher frequencies may be relevant to extreme systems with planets in very eccentric orbits. For $|\bar{\sigma}| < 0.25$ the resonance spectrum of prograde and retrograde high radial order g-modes becomes so dense that in Fig. 4 it can no longer be resolved. For decreasing forcing frequency $|\bar{\sigma}|$ the radial wavelength of the g-modes decreases, so that the resonances fade away by severe radiative damping. Also the tidal coupling strength ζ_1 of (especially the retrograde) g-modes declines with $|\bar{\sigma}|$ (see Fig. 2c). For the high frequency g-mode resonances turbulent viscosity in the (lower part) of the convective envelope provides the dominant damping. The turnover to predominant radiative damping occurs near $|\bar{\sigma}| \simeq 0.1$.

We have zoomed in to determine the resonances with the stellar normal modes down to the (somewhat arbitrary) frequency where the resonances become too weak to trace down individually.

For the prograde g-modes the resonance peaks beyond about g_{480} at $\bar{\sigma} \simeq 0.03$ ($1/x \simeq 0.15$) have been ignored, while on the retrograde side of corotation g-modes with up to about 800 radial nodes have been identified.

The off-resonant torque values follow a curved line which reflects two main effects: for high oscillation frequencies $|\bar{\sigma}|$ the turbulent dissipation in the convective envelope becomes less efficient due to the mismatch of the low frequency turbulent motions and the high frequency oscillations (Sect. 3.3), reducing the off-resonant torque-values. On the other hand, for low oscillation frequencies $|\bar{\sigma}| < 0.1$ the peak torque-values decrease strongly by the combined effect of enhanced radiative damping and the rotational confinement of the g-mode response to regions close to the stellar equator.

When we increase the (uncertain) turbulent viscosity in the convective envelope by an order of magnitude the off-resonant torque values *increase* by roughly an order of magnitude, while the peak values at the resonances (for $|\bar{\sigma}| > 0.1$ where radiative damping is weaker) *decrease* by a

similar factor. For low forcing frequencies the tidal g-mode response has short radial wavelength, and the resonances are predominantly damped by radiative damping (for the adopted turbulent viscosity law).

For $\Omega_s = 0.1$ the torque distribution (Fig. 4) shows a dip near $\bar{\sigma} \simeq -0.11$. The same dip occurs more prominently at about the same value of $1/x \simeq -0.5$ for $\Omega_s = 0.2$ (or higher rates), see Fig. 5. When the convective envelope is artificially removed from the star the dip in the torque distribution disappears. This indicates the dip is related to rotation and is caused by the convective envelope.

For frequencies $-\Omega_s/3 < \bar{\sigma} < 0$ the eigenvalues λ_1 are small (see Fig. 2a). These small eigenvalues are associated with the closely spaced quasi-toroidal q-modes which can be ordered as q_k , with k denoting the number of radial nodes. Because of the long wavelength of the lower radial order q-modes these retrograde oscillations are weakly damped. They couple efficiently to the $l = m = 2$ dominant tidal component: the angular overlap integral ζ_1 is relatively large, except when $|x|^{-1} \rightarrow 0$. In Fig. 4 and 5 the $\simeq 530$ identified q-mode resonances are not individually resolved and produce the black peak situated just left of corotation ($\bar{\sigma} = 0$). Although the damping of especially the low radial order (with small λ) oscillations of this type may be underestimated by our simple treatment, the several hundred relatively weakly damped resonances with q-modes provide a significant tidal effect by which a rapidly spinning solar-type star can be spun down efficiently.

6.6. Torque spectra for $\lambda_1 < 0$ (inertial modes)

For negative values of the eigenvalue λ_1 the corresponding tidal oscillations are restricted to the convective envelope (in contrast to all other oscillation modes considered here, which are all limited to the radiative stellar core) and are associated with a spectrum of rotationally governed inertial modes. These oscillation modes with frequencies limited to the inertial range ($|\bar{\sigma}| < 2\Omega_s$) produce an extended, relatively high torque level including a strong resonance peak (broadened by the turbulent viscosity) in the frequency range where the torque due to retrograde g-modes falls off sharply, filling the gap left of the q-modes: compare Figs. 6 and 4. The height of the inertial torque peak increases with the stellar rotation rate Ω_s and decreases when the turbulent viscosity is increased. Outside the strong resonance peak the torque-values increase with increasing viscosity. For the low-frequencies in the inertial range the value of the reduction factor in the expression for the turbulent viscosity coefficient Eq. (18) is practically equal to unity. The relatively strong inertial response can be an important driving factor for the establishment of resonance locking (WS99a; WS99b; WS01).

7. Conclusions

We have calculated the tidal torque on a rotating 1 M_⊙ star due to an orbiting companion, using the traditional

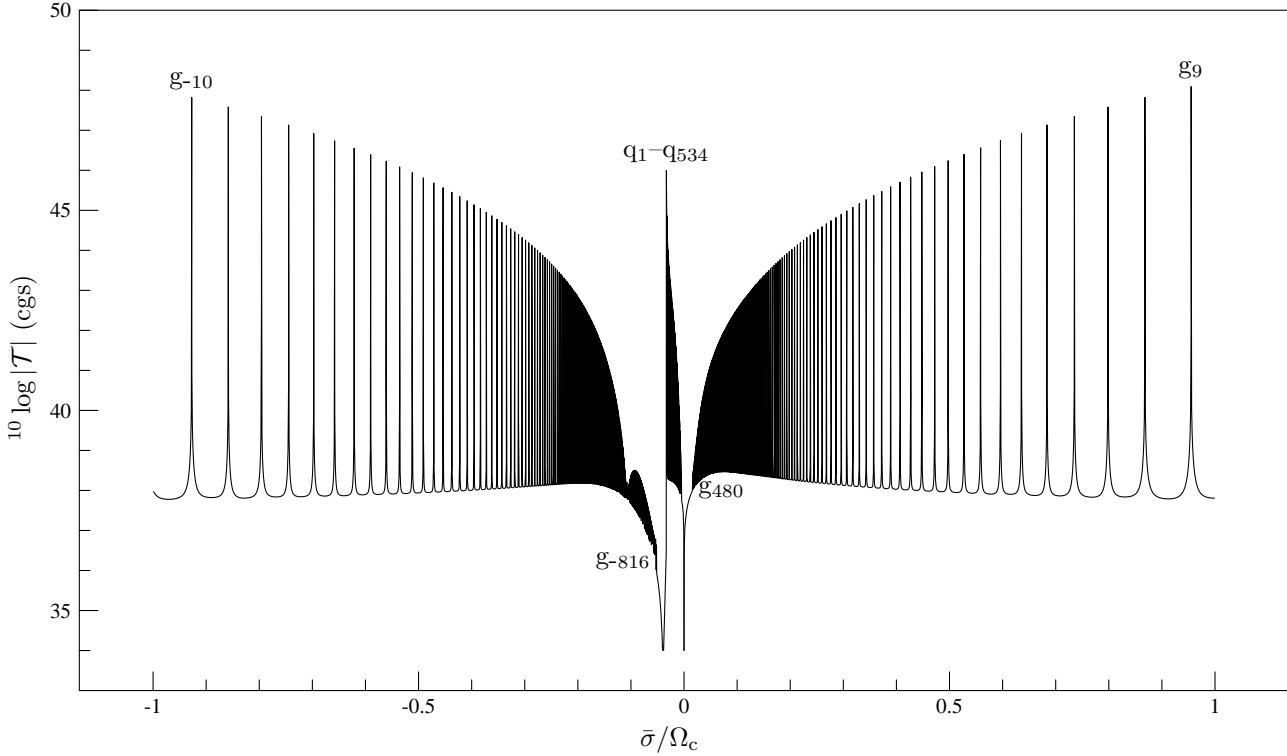


Fig. 4. The torque integral \mathcal{T} versus forcing frequency $\bar{\sigma}$ for $\lambda_1 > 0$. The calculation is for a $1 M_{\odot}$ star with central hydrogen abundance $X_c = 0.4$, rotating at speed $\Omega_s = 0.1 \Omega_c$. The narrow dip before each (low order) resonance peak has been ignored in this plot. Negative values of $\bar{\sigma}$ correspond to retrograde forcing, for which the sign of the torque should be read as negative. Results are for a fixed ratio of orbital separation to radius $D/R_s = 4$ and companion mass $M_p = 1 M_{\odot}$. Many strong resonances with quasi-toroidal q-modes, shown here as an unresolved black peak just left of $\bar{\sigma} = 0$, can be identified (with up to $\simeq 500$ radial nodes) for this stellar model.

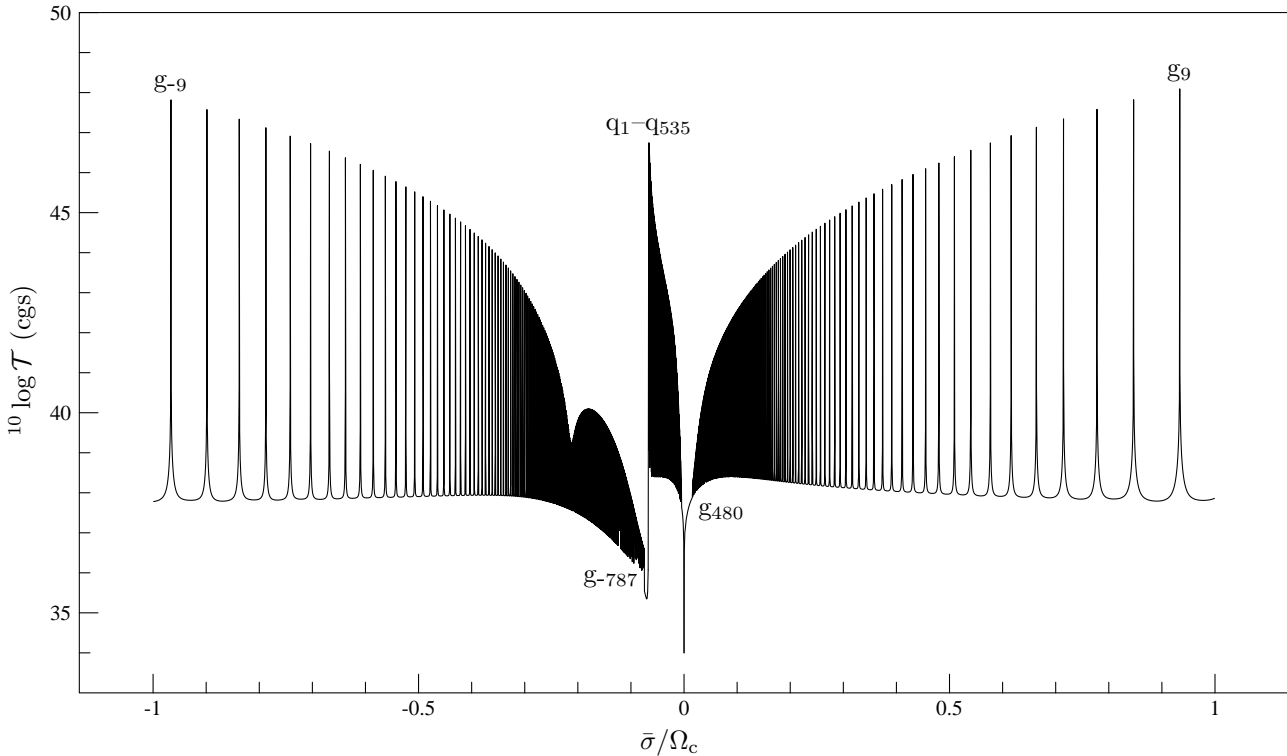


Fig. 5. The torque integral versus forcing frequency for $\lambda_1 > 0$. Same as Fig. 4, but now for rotation rate $\Omega_s = 0.2 \Omega_c$.

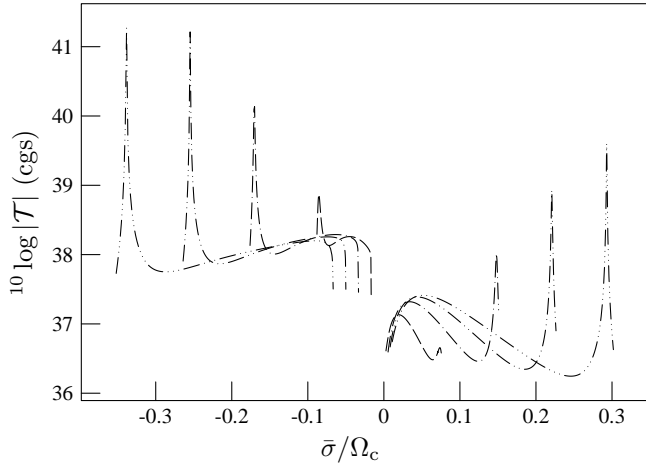


Fig. 6. The tidal torque integral versus forcing frequency for $\lambda_1 < 0$, (i.e. due to excitation of inertial modes in the convective envelope) for several stellar rotation speeds: $\Omega_s = 0.05, 0.10, 0.15$ and 0.20 in units of Ω_c . The dashed lines correspond to $\Omega_s=0.05$, the dot-dashed lines to 0.10 etc. The companion mass is $1 M_{\odot}$, while the ratio $D/R_s = 4$ was again fixed.

approximation. We have been able to identify both g-mode and quasi-toroidal q-mode resonances with up to $\simeq 1000$ radial nodes in the more evolved main sequence models by using 5000 meshpoints for the radial grid and calculated the corresponding tidal torque spectra for stellar models up to the end of core hydrogen burning. The tidal torques calculated in this paper are based on a standard local mixing length approximation for turbulent convection in the convective envelope of solar-type stars, with a simple prescription for reduced viscous damping at high forcing frequencies. The resonances with low radial order tidal oscillations are damped predominantly by the turbulent viscosity in the lower convective envelope, and the corresponding peak values for the tidal torque are inversely proportional to the adopted coefficient of turbulent viscosity. Radiative diffusion in the radial direction is also contributing to the tidal torque (strong radiative diffusion dominates the damping of resonances with high radial order g-modes at low forcing frequencies which results in weak tidal torques).

For low retrograde forcing frequencies we find a relatively strong tidal response in the convective envelope for angular eigenvalues $\lambda_1 < 0$, which corresponds to turbulent dissipation of tidally excited inertial modes. This spectrum of inertial modes may provide an efficient driving mechanism for tidal resonance locking and may generate an enhanced tidal evolution in low-mass binary systems.

For still smaller $|\bar{\sigma}|$ resonances with the retrograde quasi-toroidal q-modes (propagating in the radiative core) become a prominent feature in the torque spectrum. This q-mode spectrum consists of several hundred strong, closely spaced resonances. When the binary parameters and stellar rotation rate are such that a low orbital har-

monic falls in the frequency regime of the q-modes, enhanced tidal evolution must occur when the harmonic evolves through the many closely spaced q-mode resonances.

The effects mentioned above are related to rotation of the binary components and have been ignored in previous studies of tidal effects in low-mass binary systems. In a forthcoming paper we will apply the above results to study the tidal evolution of low-mass eccentric binary systems.

References

- Claret, A. and Cunha, N. C. S.: 1997, *A&A* **318**, 187
 Cowling, T. G.: 1941, *MNRAS* **101**, 367
 Duquennoy, A. and Mayor, M.: 1991, *A&A* **248**, 485
 Eggleton, P. P.: 1972, *MNRAS* **156**, 361
 Goldman, I. and Mazeh, T.: 1991, *ApJ* **376**, 260
 Goldreich, P. and Keeley, D. A.: 1977, *ApJ* **211**, 934
 Goodman, J. and Dickson, E. S.: 1998, *ApJ* **507**, 938
 Goodman, J. and Oh, S. P.: 1997, *ApJ* **486**, 403
 Iglesias, C. A. and Rogers, F. J.: 1996, *ApJ* **464**, 943
 Latham, D. W., Mazeh, T., Stefanik, R. P., Davis, R. J., Carney, B. W., Krymowski, Y., Laird, J. B., Torres, G., and Morse, J. A.: 1992, *AJ* **104**, 774
 Mathieu, R. D., Duquennoy, A., Latham, D. W., Mayor, M., Mermilliod, T., and Mazeh, J. C.: 1992, in *Binaries as tracers of stellar formation. A. Duquennoy and M. Mayor (eds)*, p. 278, Cambridge University Press
 Papaloizou, J. and Pringle, J. E.: 1978, *MNRAS* **182**, 423
 Papaloizou, J. C. B. and Savonije, G. J.: 1997, *MNRAS* **291**, 651
 Pols, O. R., Tout, C. A., Eggleton, P. P., and Han, Z.: 1995, *MNRAS* **274**, 964
 Press, W. H., Teukolsky, S. A., Vetterling, W. T., and Flannery, B. P.: 1992, *Numerical recipes in FORTRAN. The art of scientific computing, 2nd ed.*, Cambridge University Press
 Savonije, G. J. and Papaloizou, J. C. B.: 1983, *MNRAS* **203**, 581
 Savonije, G. J. and Papaloizou, J. C. B.: 1997, *MNRAS* **291**, 633
 Savonije, G. J., Papaloizou, J. C. B., and Alberts, F.: 1995, *MNRAS* **277**, 471
 Terquem, C., Papaloizou, J. C. B., Nelson, R. P., and Lin, D. N. C.: 1998, *ApJ* **502**, 788
 Unno, W., Osaki, Y., Ando, H., Saio, H., and Shibahashi, H.: 1989, *Nonradial oscillations of stars*, Univ. of Tokyo Press
 Verbunt, F. and Phinney, E. S.: 1995, *A&A* **296**, 709
 Witte, M. G. and Savonije, G. J.: 1999a, *A&A* **341**, 842
 Witte, M. G. and Savonije, G. J.: 1999b, *A&A* **350**, 129
 Witte, M. G. and Savonije, G. J.: 2001, *A&A* **366**, 840
 Zahn, J. P.: 1977, *A&A* **57**, 383